Global Journal of Pure and Applied Mathematics.
ISSN 0973-1768 Volume 19, Number 1 (2023), pp. 43-65

http://www.ripublication.com/gjpam.htm

Heat and Mass Transfer in Hydromagnetic Nanofluid Convective Flow Through Artificial Kidney Past Porous Stretching Cylinder under the Effects of Thermal Conductivity

Christopher Venance*[1], Mathew N. Kinyanjui [2], and Kang'ethe Giterere[3]

[1]*Department of Mathematics, Pan African University Institute for Basic Sciences Technology and Innovation (PAUSTI), Nairobi, Kenya.*
[2]*Department of Pure and Applied Mathematics, Jomo Kenyatta University of Agriculture and Technology (JKUAT), Nairobi, Kenya.*
[3]*Department of Pure and Applied Mathematics, Jomo Kenyatta University of Agriculture and Technology (JKUAT), Nairobi, Kenya.*

Abstract

The study of mass and heat transfer in hydromagnetic nanofluid convective flow through hollow fibers in an artificial kidney past a porous stretching cylinder under the effects of thermal conductivity has been considered. In an artificial kidney, the flow of nanofluid is assumed to be axis-symmetrical. The flow is unsteady and a magnetic field is transversely applied to the porous cylinder as dialyzer in the artificial kidney. The aim of the study includes the application of nanometer-sized particles into the basefluid with the aim of enhancing its thermo-physical properties such as thermal conductivity, viscosity, convective heat transfer and diffusivity. The flow governing equations are coupled and nonlinear, the equations are solved by a finite-difference method that applies Crank-Nicolson techniques, and the results obtained are presented graphically followed by a discussion of the findings. It is observed that the application of nanoparticles into base fluid improve dialysis sessions during the filtration of a patient's blood in an artificial kidney from a minimum of eight hours to two hours. The effects of the various non-dimensional parameters on the skin friction coefficient, Sherwood, and Nusselt numbers have been presented in tabular form. It is noted that as time decreases, skin friction at the surface of the stretching cylinder decreases, while Sherwood and Nusselt numbers increase.

Keywords: Thermal conductivity, nanoparticles, stretching cylinder, heat transfer, mass transfer, Artificial kidney.

*Corresponding Author.

1. INTRODUCTION

One of the thermo-physical characteristics of base fluid used to measure convective heat transfer via a porous stretching cylinder during hemodialysis in an artificial kidney is thermal conductivity. In order to demonstrate how thermal conductivity in a blood flow problem can improve the motion of solutes from blood to the dialysis solution compartment via the pores present in the hollow fiber membrane in an artificial kidney, metallic nanoparticles are suspended in the base fluid to form nanofluid. Several numerical and mathematical models on the effects of thermal conductivity past a porous stretching cylinder have been established such as [1] established a mathematical model on heat transfer and thermal conductivity of magneto-micropolar fluid moving through vertical porous medium under thermal non-equilibrium conditions. A mathematical model of Eyring-Powell nanofluid flow with non-linear radiation, variable thermal conductivity, and viscosity was established by [15], [27]. [8] carried out a mathematical model on Blasius-Rayleigh Stokes flow and heat transfer over a moving plate affected by thermal conductivity when the magnetic dipole moment is taken into account. Variable viscosity and thermal conductivity have an impact on the dynamics of MHD cross nanofluid over a stratified Darcy-Forchheimer porous surface of a paraboloid of revolution subjected to entropy production studied by, [21]. [30] studied on Performance of thermal conductivity in SWCNTs-CuO/Ethylene Glycol hybrid nanofluid flow: dual solutions. [5] established a mathematical model on the cylindrical moving boundary problem with changing thermal conductivity and convection under the most plausible boundary conditions.

The frictional forces at the walls of the stretching cylinder are significantly influenced by the study of the boundary layers. The area where surface friction, convective heat, and mass transfer in fluids are measured is known as the boundary layer, and this fact has direct practical significance. Applications for boundary layers in a stretching cylinder in biomedical engineering include designing blood pumping devices, peristaltic plasma pumping, controlling cooling boundary layers, controlling gaseous diffusion, and designing modern artificial kidney devices. Based on these applications, [7] studied the impact of heat generation absorption on the boundary layer flow of a nanofluid containing gyrotactic microorganisms over an inclined stretching cylinder. A mathematical model on flow of a hybrid nanofluid across a moving plate using magnetohydrodynamics (MHD) and Joule heating by, [13]. [23] examined the boundary layer stagnation point, heat transport over coupled-stress fluid flow over an exponentially stretched sheet was examined. The Buongiorno nanofluid model was used to do a mathematical computation for the boundary layer flow of viscoelastic fluid toward a nonlinear stretching cylinder by, [17]. [2] studied a thermal model for the bio-convection transport of nanofluids generated by stretching cylinders with Marangoni boundary conditions. [26] Analysed heat transfer stability in boundary layer flow of a hybrid nanofluid versus a nanofluid in the direction of a diminishing surface.

Recently, the study of heat and mass transfer has attracted many researchers. Numerous studies have focused on the mass and heat transfer of hydromagnetic convective nanofluid flow over a stretching cylinder, with the application involving fluids, chemical reactions, and the rate at which solutes diffuse through pores of hollow fibers in an artificial kidney, such as heat exchangers, blood oxygenators, and blood flow in the capillaries. [20] analysed heat and mass transport in a nanofluid flow through a rotating cylinder using the Cattaneo-Christov heat flux. Analysis of heat and mass transmission over a non-uniform infinite porous surface with chemical reactions by, [4]. A study on the effects of chemical reaction and viscous dissipation in MHD heat and mass transfer nanofluid flow on a porous stretching cylinder by, [22]. [16], [12] analyzed the properties of heat and mass transfer in a nanofluid flow over an exponentially stretchable sheet with activation energy. Also, [28] analyzed the nonlinear mixed-convective hybrid nanofluid flow's heat and mass transfer under various slip boundary conditions.

Nanoparticle is a small particle of matter made up of metals, oxides, nitrides, or carbides having very small diameters ranges between $(1nm)$ to $(100nm)$, undetectable by the human eye, and can exhibit significantly different physical and chemical properties to their larger material counterparts. In past decades, nanotechnology has played an important role in biomedical engineering with the application of nanoparticles into the base fluid to form nanofluid with the aim of improving the thermal conductivity of the base fluid by, [18], [3]. [31] carried out a study on the applications of nanofluids in enhancing thermal conductivity. Enhancing natural convective heat transfer around a spherical structure by applying micropolar nanofluid in a magnetic field developed by, [29] . [11] established a mathematical model on MoS4 and copper nanoparticles suspended in magnetic hybrid nanoparticles with a stretching/shrinking cylinder. Effect of nanoparticle shape on heat transfer efficiency of magnetized ternary hybrid nanofluids through a porous stretched cylinder studied by, [24]. The numerical simulation of nanoparticle size and thermal radiation with the effect of magnetic field based on tangent hyperbolic fluid flow was developed by, [14].
In biomedical engineering, an artificial kidney can be used in the designing of blood pumping devices, peristaltic plasma pumping systems, and contemporary artificial kidney machines. Recent research has been focused on designing an optimal artificial kidney that improves the lives and prolongs the survival of patients with two natural kidney problems. Design of a contemporary artificial kidney with dialysis membranes for blood purification by, [9] [25]. [32] developed a mathematical model with widened interlayer spacing and MoS2 nanosheets with highly effective uremic toxin adsorption for urea-free wearable artificial kidneys. [19] established models of Mass Transfer in Membrane Processes: Use in Artificial Organs. [6] studied how cretinine is filtered through a nanofibrous membrane in a transportable artificial kidney during blood dialysis. A strategy for using graphene that has been doped with nitrogen and phosphorus to enhance the removal of urea in a wearable dialysis device for patients with end-stage renal illness developed by, [10].

In the literature cited, no studies have been done on mass and heat transfer in hydromagnetic nanofluid convective flow through artificial kidneys past a porous stretching cylinder under the effects of thermal conductivity. The goal of the present investigation involves the application of nanoparticles into the base fluid that improve the thermal conductivity of the base fluid so that it can provide significant continuous blood purification of metabolic waste products and toxins from blood to dialysis solution by improving dialysis sessions, which improves the quality of life of the natural kidney for patients.

2. MATHEMATICAL MODEL FORMULATION

A mathematical model governing the mass and heat transfer in hydromagnetic nanofluid convective flow through an artificial kidney past a porous stretching cylinder under the effects of thermal conductivity is formulated. The flow of blood through the hollow fibers in an artificial kidney is assumed to be axis-symmetrical, and the flow is considered laminar. Stretching cylinder with hollow fibers membrane is permeable to allow solutes from blood to diffuse through semi-permeable membrane to dialysis solution compartment in an artificial kidney by diffusion method. In Figure (1) the surface of the stretching cylinder is kept at a temperature higher than the free-stream i.e $T_{R_1} > T_{R_2}$ an upward flow is established along the surface due to natural convection. The concentration of the nanofluid is greater than the surrounding concentration i.e $C_{R_1} > C_{R_2}$. The magnetic field B_0 is applied perpendicular to the permeable and impermeable cylinders.

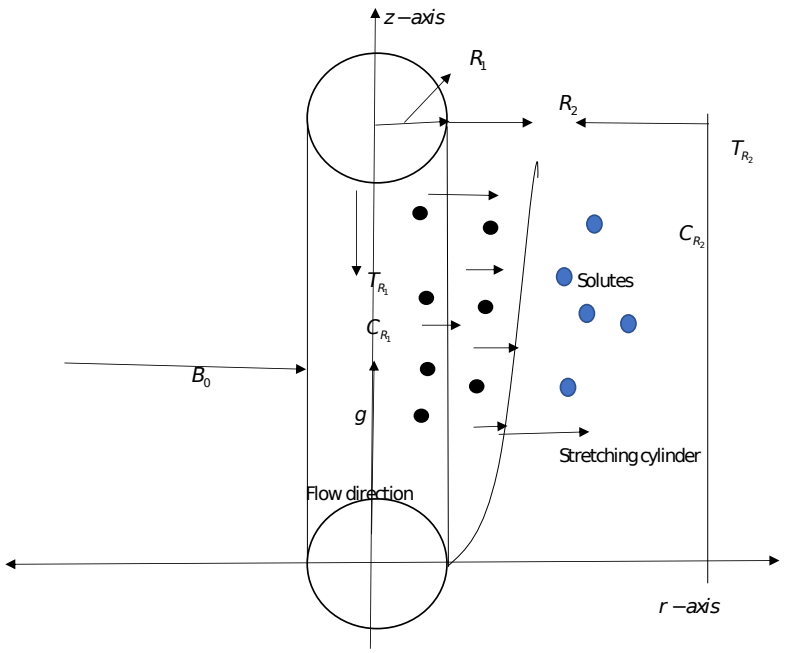

Figure 1: Flow problem geometry

2.1. Flow governing equations

The continuity, momentum, energy, and concentration equations that govern heat and mass transfer in nanofluid past a porous stretching cylinder with the effect of thermal conductivity are given in cylindrical polar coordinates as follows.

$$\frac{1}{r}\frac{\partial}{\partial r}\left(w_r\right)+\frac{1}{r}\frac{\partial}{\partial \theta}\left(w_\theta\right)+\frac{\partial}{\partial z}\left(w_z\right)=0 \tag{1}$$

$$\frac{\partial w_z}{\partial t}+w_r\frac{\partial w_z}{\partial r}+w_z\frac{\partial w_z}{\partial z}=\nu\left(\frac{1}{r}\frac{\partial w_z}{\partial r}+\frac{\partial^2 w_z}{\partial r^2}\right)+\nu\frac{\partial^2 w_z}{\partial z^2}-\frac{\nu}{K_p}w_z-\frac{\sigma w_z B_0^2}{\rho_{nf}} +\beta_T g\left(T-T_{R_2}\right)+\beta_C g\left(C-C_{R_2}\right) \tag{2}$$

and

$$\frac{\partial w_r}{\partial t}+w_r\frac{\partial w_r}{\partial r}+w_z\frac{\partial w_r}{\partial z}=\nu\left(\frac{1}{r}\frac{\partial w_r}{\partial r}+\frac{\partial^2 w_r}{\partial r^2}\right)+\nu\frac{\partial^2 w_r}{\partial z^2}-\nu\frac{w_r}{r^2}-\frac{\nu}{K_p}w_r-\frac{\sigma w_r B_0^2}{\rho_{nf}} \tag{3}$$

$$\left(\rho C_p\right)_{nf}\left(\frac{\partial T}{\partial t}+w_r\frac{\partial T}{\partial r}+w_z\frac{\partial T}{\partial z}\right)=$$

$$k_{nf}\left(\frac{1}{r}\frac{\partial T}{\partial r}+\frac{\partial^2 T}{\partial r^2}+\frac{\partial^2 T}{\partial z^2}\right)+2\mu_{nf}\left[\left(\frac{\partial w_r}{\partial r}\right)^2+\left(\frac{w_r}{r}\right)^2+\left(\frac{\partial w_z}{\partial z}\right)^2\right] +\mu_{nf}\left[\left(\frac{\partial w_z}{\partial r}+\frac{\partial w_r}{\partial z}\right)^2\right]+\sigma B_0^2 w_z^2+S_T\left(T-T_{R_2}\right) \tag{4}$$

$$\frac{\partial C}{\partial t}+w_r\frac{\partial C}{\partial r}+w_z\frac{\partial C}{\partial z}=D_m\left[\frac{\partial^2 C}{\partial r^2}+\frac{1}{r}\frac{\partial C}{\partial r}+\frac{\partial^2 C}{\partial z^2}\right] +\alpha_{nf}\left(\frac{\partial^2 T}{\partial r^2}+\frac{1}{r}\frac{\partial T}{\partial r}+\frac{\partial^2 T}{\partial z^2}\right)+\gamma_C\left(C-C_{R_2}\right) \tag{5}$$

Initial and boundary condition, $w_r=0$, $w_z=0.5ms^{-1}$, $C=0$, $T=37K$, at $0\leq r\leq R_2$, $L=R_2-R_1$ and $R_1\leq r\leq R_2$, when $t=0$.

$w_z=Nw_z\left(z\right)$, $w_r=w_0$,

$\lim_{r\to R_2} w_r\left(R_2,z,t\right)=0$, $\lim_{r\to R_2} C\left(R_2,z,t\right)=C_{R_2}$, $\lim_{r\to R_2} T\left(R_2,z,t\right)=T_{R_2}$ at $r=R_2$

when $t > 0$.

where $w_z(z) = w_1 e^{\left(\frac{z}{L}\right)}$ is the stretching velocity. $w_0 > 0$ is the suction velocity, $w_0 < 0$ is the injection velocity.

2.2. Non-dimensionalization

The equations are non-dimensionalized using the transformations.
$w_0^\star = \frac{w_0}{w_{R_2}}$, $w_r^\star = \frac{w_r}{w_{R_2}}$, $w_z^\star = \frac{w_z}{w_{R_2}}$, $r^\star = \frac{r}{L}$, $R_1^\star = \frac{R_1}{L}$, $R_2^\star = \frac{R_2}{L}$, $t^\star = \frac{w_{R_2} t}{L}$, $z^\star = \frac{z}{L}$, $T^\star = \frac{T - T_{R_2}}{T_{R_1} - T_{R_2}}$, $C^\star = \frac{C - C_{R_2}}{C_{R_1} - C_{R_2}}$
where, w_{R_2}, L, C and T are the characteristics velocity, length, concentration and temperature.
The final equations of motion, Temperature and concentration in non-dimensional form.

$$\frac{\partial w_z^\star}{\partial t^\star} + w_r^\star \frac{\partial w_z^\star}{\partial r^\star} + w_z^\star \frac{\partial w_z^\star}{\partial z^\star} = \frac{1}{Re}\left(\frac{1}{r^\star}\frac{\partial w_z^\star}{\partial r^\star} + \frac{\partial^2 w_z^\star}{\partial r^{\star 2}} + \frac{\partial^2 w_z^\star}{\partial z^{\star 2}}\right) - \lambda_p w_z^\star - M w_z^\star + G_{rT} T^\star + G_{rC} C^\star \tag{6}$$

and

$$\frac{\partial w_r^\star}{\partial t^\star} + w_r^\star \frac{\partial w_r^\star}{\partial r^\star} + w_z^\star \frac{\partial w_r^\star}{\partial z^\star} = \frac{1}{Re}\left(\frac{1}{r^\star}\frac{\partial w_r^\star}{\partial r^\star} + \frac{\partial^2 w_r^\star}{\partial r^{\star 2}} + \frac{\partial^2 w_r^\star}{\partial z^{\star 2}}\right) - \frac{w_r^\star}{Re r^{\star 2}} - \lambda_p w_r^\star - M w_r^\star \tag{7}$$

$$\left(\frac{\partial T^\star}{\partial t^\star} + w_r^\star \frac{\partial T^\star}{\partial r^\star} + w_z^\star \frac{\partial T^\star}{\partial z^\star}\right) = \frac{1}{PrRe}\left(\frac{1}{r^\star}\frac{\partial T^\star}{\partial r^\star} + \frac{\partial^2 T^\star}{\partial r^{\star 2}} + \frac{\partial^2 T^\star}{\partial z^{\star 2}}\right) + \frac{2Ec}{Re}\left[\left(\frac{\partial w_r^\star}{\partial r^\star}\right)^2 + \left(\frac{w_r^\star}{r^\star}\right)^2 + \left(\frac{\partial w_z^\star}{\partial z^\star}\right)^2\right] + \frac{Ec}{Re}\left[\left(\frac{\partial w_z^\star}{\partial r^\star}\right)^2 + 2\left(\frac{\partial w_z^\star}{\partial r^\star}\right)\left(\frac{\partial w_r^\star}{\partial z^\star}\right) + \left(\frac{\partial w_r^\star}{\partial z^\star}\right)^2\right] + \frac{H_J}{Re} w_z^{\star 2} + \frac{S}{Re} T^\star \tag{8}$$

$$\frac{\partial C^\star}{\partial t^\star} + w_r^\star \frac{\partial C^\star}{\partial r^\star} + w_z^\star \frac{\partial C^\star}{\partial z^\star} = \frac{Sc}{Re}\left(\frac{1}{r^\star}\frac{\partial C^\star}{\partial r^\star} + \frac{\partial^2 C^\star}{\partial r^{\star 2}} + \frac{\partial^2 C^\star}{\partial z^{\star 2}}\right) + \frac{Sr}{Re}\left(\frac{1}{r^\star}\frac{\partial T^\star}{\partial r^\star} + \frac{\partial^2 T^\star}{\partial r^{\star 2}} + \frac{\partial^2 T^\star}{\partial z^{\star 2}}\right) + \frac{\gamma}{Re} C^\star \tag{9}$$

Initial and boundary conditions in non-dimensional form. $w_r^\star = 0$, $w_z^\star = 0.5ms^{-1}$, $C^\star = 0$, $T^\star = 37K$, at $0 \leq r^\star \leq \dfrac{R_2}{L}$, $L = R_2 - R_1$ and $\dfrac{R_1}{L} \leq r^\star \leq \dfrac{R_2}{L}$.

$w_z^\star = N\left(\dfrac{w_1}{w_{R_2}}e^{z\star}\right)$, $w_r^\star = w_0^\star w_{R_2}$, for any value of z.

$z^\star = \infty$, $w_r^\star = 1$, $w_z^\star = 1$, $C^\star = 1$, $T^\star = 1$,
$\lim\limits_{r^\star \to \frac{R_2}{L}} w_r^\star\left(\dfrac{R_2}{L}, z, t\right) = 0$, $\lim\limits_{r^\star \to \frac{R_2}{L}} C^\star\left(\dfrac{R_2}{L}, z, t\right) = 1$, $\lim\limits_{r^\star \to \frac{R_2}{L}} T^\star\left(\dfrac{R_2}{L}, z, t\right) = 1$ at
$r^\star = \dfrac{R_2}{L}$ when $t^\star > 0$,

2.3. Numerical methods

Numerical techniques for solving differential equations by approximating derivatives with finite differences that apply Crank-Nicolson techniques. The equations governing mass and heat transfer in hydromagnetic nanofluid convective flow through an artificial kidney past a porous stretching cylinder under the effects of thermal conductivity are highly coupled and non-linear. The finite difference equations for the velocity, temperature, and concentration profiles are given by

$$w_{z_{i,j}}^{m+1} = [w_{z_{i,j}}^m - \frac{w_{r_{i,j}}^m \Delta t}{2(\Delta r)}\left(-w_{z_{i-1,j}}^{m+1} + w_{z_{i,j}}^m - w_{z_{i-1,j}}^m\right)$$

$$-\frac{w_{z_{i,j}}^m \Delta t}{2(\Delta z)}\left(-w_{z_{i,j-1}}^{m+1} + w_{z_{i,j}}^m - w_{z_{i,j-1}}^m\right) + \frac{\Delta t}{2rRe(\Delta r)}\left(-w_{z_{i-1,j}}^{m+1} + w_{z_{i,j}}^m - w_{z_{i-1,j}}^m\right)$$

$$+\frac{\Delta t}{2Re(\Delta r)^2}\left(w_{z_{i+1,j}}^{m+1} + w_{z_{i-1,j}}^{m+1} + w_{z_{i+1,j}}^m - 2w_{z_{i,j}}^m + w_{z_{i-1,j}}^m\right)$$

$$+\frac{\Delta t}{2Re(\Delta z)^2}\left(w_{z_{i,j+1}}^{m+1} + w_{z_{i,j-1}}^{m+1} + w_{z_{i,j+1}}^m - 2w_{z_{i,j}}^m + w_{z_{i,j-1}}^m\right)$$

$$-\Delta t\frac{\lambda_p}{2}w_{z_{i,j}}^m - \Delta t\frac{M}{2}w_{z_{i,j}}^m$$

$$+\Delta t\frac{G_{rT}}{2}\left(T_{i,j}^{m+1} + T_{i,j}^m\right) + \Delta t\frac{G_{rC}}{2}\left(C_{i,j}^{m+1} + C_{i,j}^m\right)]$$

$$/[1+\frac{w_{r_i,j}^m\Delta t}{2\left(\Delta r\right)}+\frac{w_{z_i,j}^m\Delta t}{2\left(\Delta z\right)}-\frac{\Delta t}{2rRe\left(\Delta r\right)}+\frac{\Delta t}{Re\left(\Delta r\right)^2}+\frac{\Delta t}{Re\left(\Delta z\right)^2}+\frac{\lambda_p\Delta t}{2}+\frac{M\Delta t}{2}] \tag{10}$$

$$w_{r_i,j}^{m+1}=[w_{r_i,j}^m-\frac{w_{r_i,j}^m\Delta t}{2\left(\Delta r\right)}\left(-w_{r_{i-1,j}}^{m+1}+w_{r_i,j}^m-w_{r_{i-1,j}}^m\right)$$

$$-\frac{w_{z_i,j}^m\Delta t}{2\left(\Delta z\right)}\left(-w_{r_{i,j-1}}^{m+1}+w_{r_i,j}^m-w_{r_{i,j-1}}^m\right)+\frac{\Delta t}{2rRe\left(\Delta r\right)}\left(-w_{r_{i-1,j}}^{m+1}+w_{r_i,j}^m-w_{r_{i-1,j}}^m\right)$$

$$+\frac{\Delta t}{2Re\left(\Delta r\right)^2}\left(w_{r_{i+1,j}}^{m+1}+w_{r_{i-1,j}}^{m+1}+w_{r_{i+1,j}}^m-2w_{r_i,j}^m+w_{r_{i-1,j}}^m\right)$$

$$+\frac{\Delta t}{2Re\left(\Delta z\right)^2}\left(w_{r_{i,j+1}}^{m+1}+w_{r_{i,j-1}}^{m+1}+w_{r_{i,j+1}}^m-2w_{r_i,j}^m+w_{r_{i,j-1}}^m\right)-\frac{\Delta t}{2Rer^2}w_{r_i,j}^m$$

$$-\Delta t\frac{\lambda_p}{2}w_{r_i,j}^m-\Delta t\frac{M}{2}w_{r_i,j}^m]/[1$$

$$+\frac{w_{r_i,j}^m\Delta t}{2\left(\Delta r\right)}+\frac{w_{z_i,j}^m\Delta t}{2\left(\Delta z\right)}-\frac{\Delta t}{2\left(\Delta r\right)rRe}$$

$$+\frac{\Delta t}{2r^2Re}+\frac{\Delta t}{Re\left(\Delta r\right)^2}+\frac{\Delta t}{Re\left(\Delta z\right)^2}+\frac{\lambda_p\Delta t}{2}+\frac{M\Delta t}{2}] \tag{11}$$

$$T_{i,j}^{m+1}=[T_{i,j}^m-\frac{w_{r_i,j}^m\Delta t}{2\left(\Delta r\right)}\left(-T_{i-1,j}^{m+1}+T_{i,j}^m-T_{i-1,j}^m\right)-\frac{w_{z_i,j}^m\Delta t}{2\left(\Delta z\right)}\left(-T_{i,j-1}^{m+1}+T_{i,j}^m-T_{i,j-1}^m\right)$$

$$+\frac{\Delta t}{2rRePr\left(\Delta r\right)}\left(-T_{i-1,j}^{m+1}+T_{i,j}^m-T_{i-1,j}^m\right)$$

$$+\frac{\Delta t}{2RePr\left(\Delta r\right)^2}\left(T_{i+1,j}^{m+1}+T_{i-1,j}^{m+1}+T_{i+1,j}^m-2T_{i,j}^m+T_{i-1,j}^m\right)$$

$$+\frac{\Delta t}{2RePr\left(\Delta z\right)^2}\left(T_{i,j+1}^{m+1}+T_{i,j-1}^{m+1}+T_{i,j+1}^m-2T_{i,j}^m+T_{i,j-1}^m\right)$$

$$+\frac{Ec\Delta t}{2Re\left(\Delta r\right)^2}\left(w_{r_i,j}^{m+1}-w_{r_{i-1,j}}^{m+1}+w_{r_i,j}^m-w_{r_{i-1,j}}^m\right)^2$$

$$+\frac{Ec\Delta t}{Rer^2}\left(w_{r_{i,j}}^{m+1}+w_{r_{i,j}}^{m}\right)^2+\frac{Ec\Delta t}{2Re\left(\Delta z\right)^2}\left(w_{z_{i,j}}^{m+1}-w_{z_{i,j-1}}^{m+1}+w_{z_{i,j}}^{m}-w_{z_{i,j-1}}^{m}\right)^2$$

$$+\frac{Ec\Delta t}{4Re\left(\Delta r\right)^2}\left(w_{z_{i,j}}^{m+1}-w_{z_{i-1,j}}^{m+1}+w_{z_{i,j}}^{m}-w_{z_{i-1,j}}^{m}\right)^2$$

$$+\frac{Ec\Delta t}{2Re\left(\Delta r\right)\left(\Delta z\right)}\left(w_{z_{i,j}}^{m+1}-w_{z_{i-1,j}}^{m+1}+w_{z_{i,j}}^{m}-w_{z_{i-1,j}}^{m}\right)$$

$$\times\left(w_{r_{i,j}}^{m+1}-w_{r_{i,j-1}}^{m+1}+w_{r_{i,j}}^{m}-w_{r_{i,j-1}}^{m}\right)+\frac{Ec\Delta t}{4Re\left(\Delta z\right)^2}\left(w_{r_{i,j}}^{m+1}-w_{r_{i,j-1}}^{m+1}+w_{r_{i,j}}^{m}-w_{r_{i,j-1}}^{m}\right)^2$$

$$+\Delta t\frac{H_J}{2Re}\left(w_{z_{i,j}}^{m+1}+w_{z_{i,j}}^{m}\right)^2+\frac{S\Delta t}{2Re}T_{i,j}^{m}]/[1+\frac{w_{r_i,j}^{m}\Delta t}{2\left(\Delta r\right)}+\frac{w_{z_i,j}^{m}\Delta t}{2\left(\Delta z\right)}$$

$$-\frac{\Delta t}{2rRePr\left(\Delta r\right)}+\frac{\Delta t}{RePr\left(\Delta r\right)^2}+\frac{\Delta t}{RePr\left(\Delta z\right)^2}-\frac{S\Delta t}{2Re}] \tag{12}$$

$$C_{i,j}^{m+1}=[C_{i,j}^{m}-\frac{w_{r_i,j}^{m}\Delta t}{2\left(\Delta r\right)}\left(-C_{i-1,j}^{m+1}+C_{i,j}^{m}-C_{i-1,j}^{m}\right)-\frac{w_{z_i,j}^{m}\Delta t}{2\left(\Delta z\right)}\left(-C_{i,j-1}^{m+1}+C_{i,j}^{m}-C_{i,j-1}^{m}\right)$$

$$+\frac{\Delta t}{2r\left(\Delta r\right)ScRe}\left(-C_{i-1,j}^{m+1}+C_{i,j}^{m}-C_{i-1,j}^{m}\right)$$

$$+\frac{\Delta t}{2\left(\Delta r\right)^2ScRe}\left(C_{i+1,j}^{m+1}+C_{i-1,j}^{m+1}+C_{i+1,j}^{m}-2C_{i,j}^{m}+C_{i-1,j}^{m}\right)$$

$$+\frac{\Delta t}{2\left(\Delta z\right)^2ScRe}\left(C_{i,j+1}^{m+1}+C_{i,j-1}^{m+1}+C_{i,j+1}^{m}-2C_{i,j}^{m}+C_{i,j-1}^{m}\right)$$

$$+\frac{Sr\Delta t}{2r\left(\Delta r\right)Re}\left(T_{i,j}^{m+1}-T_{i-1,j}^{m+1}+T_{i,j}^{m}-T_{i-1,j}^{m}\right)$$

$$+\frac{Sr\Delta t}{2\left(\Delta r\right)^2Re}\left(T_{i+1,j}^{m+1}-2T_{i,j}^{m+1}+T_{i-1,j}^{m+1}+T_{i+1,j}^{m}-2T_{i,j}^{m}+T_{i-1,j}^{m}\right)$$

$$+\frac{Sr\Delta t}{2\left(\Delta z\right)^2Re}\left(T_{i,j+1}^{m+1}-2T_{i,j}^{m+1}+T_{i,j-1}^{m+1}+T_{i,j+1}^{m}-2T_{i,j}^{m}+T_{i,j-1}^{m}\right)+\frac{\gamma\Delta t}{2Re}C_{i,j}^{m}]/[1+$$

$$\frac{w_{r_i,j}^{m}\Delta t}{2\left(\Delta r\right)}+\frac{w_{z_i,j}^{m}\Delta t}{2\left(\Delta z\right)}-\frac{\Delta t}{2r\left(\Delta r\right)ScRe}+\frac{\Delta t}{\left(\Delta r\right)^2ScRe}+\frac{\Delta t}{\left(\Delta z\right)^2ScRe}-\frac{\gamma\Delta t}{2Re}] \tag{13}$$

The wall skin friction coefficient can be calculated from axial and radial velocity profiles. Laminar flow of an incompressible nanofluid has low wall skin friction that improves the nanofluid movement through the wall surface of the hollow fibers in an artificial kidney. It is given by, The wall skin friction coefficients in axial and radial direction are given as

$$C_{s_z} = \frac{2}{Re}\left[\frac{\partial w_z^\star}{\partial r^\star}\right]_{r^\star=0} \tag{14}$$

and,

$$C_{s_r} = -\frac{2}{Re}\left[\frac{\partial w_r^\star}{\partial r^\star}\right]_{r^\star=0} \tag{15}$$

The wall mass transfer rate is determined from concentration profiles. It is given by Sherwood number past a porous stretching cylinder of hollow fibers in an artificial kidney.

$$Sh_m = \frac{-\frac{D_m}{L}\left(C_{R1} - C_{R2}\right)\left[\frac{\partial C^\star}{\partial r^\star}\right]_{r^\star=0}}{\frac{D_m}{L}\left(C_{R1} - C_{R2}\right)} = -\left[\frac{\partial C^\star}{\partial r^\star}\right]_{r^\star=0} \tag{16}$$

The rate of heat transfer is determined from temperature profiles and it is given by Nusselt number.

$$Nu_w = \frac{-\frac{k_{nf}}{L}\left(T_{R1} - T_{R2}\right)\left[\frac{\partial T^\star}{\partial r^\star}\right]_{r^\star=0}}{\frac{k_{nf}}{L}\left(T_{R1} - T_{R2}\right)} = -\left[\frac{\partial T^\star}{\partial r^\star}\right]_{r^\star=0} \tag{17}$$

3. DISCUSSION OF THE RESULTS

From the findings, the effects of various non-dimensional parameters such as the Magnetic field parameter, Permeability parameter, Prandtl number and Joule heating parameter on velocity, temperature, and concentration profiles are discussed.
It is noted from Figure $2\,(a)$ that as time (t) increases, nanofluid velocity (Wz) decreases. This is due to the fact that the velocity of the nanofluid increases as time decreases during hemodialysis due to the application of nanoparticles into the base fluid. Figure $2\,(b)$ shows that as time (t) increases, radial velocity (Wr) decreases. This is to the fact that, velocity of the solutes from blood to the dialysis solution compartment through the pores of the hollow fibers increases as time decreases. It is observed from figure $2\,(c)$ that as time (t) increases, temperature (T) decreases. This is due to the fact that as time decreases, temperature increases along the stretching cylinder as the heat source and the nanoparticles dissolve into the base fluid, improving the thermal boundary layer thickness. and increases its temperature profiles and figure $2\,(d)$ shows that as time (t) increases, Concentration of the nanofluid (C) increases but as it is approaching the surface of the stretching cylinder the concentration decreases. This is due to the fact that the concentration gradient of the blood and dialysate helps the movement of the solutes from the blood to the dialysis solution compartment as time decreases. Filtration of the solutes and other metabolic products like urea, creatinine, and excess fluid that are unwanted to the patient is done from the blood into the dialysis solution compartment in the stretching cylinder as time decreases.

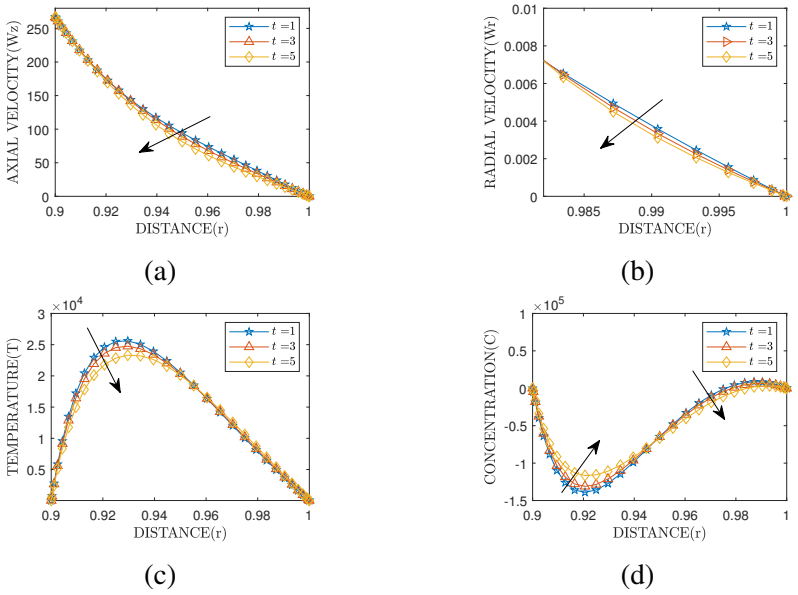

Figure 2: Effects of time (t) on Axial velocity (Wz), Radial velocity (Wr), Temperature (T) and Concentration (C) profiles

It is observed from Figure 3 (a) that, an increase in Schmidt number (Sc) results to an increase in the axial velocity (Wz). Physically, Schmidt number is the ratio of kinematic viscosity diffusivity to mass diffusivity of solutes in nanofluid. Schmidt's number increases nanofluid velocity and boundary layer thickness due to the Hall current effect, which improves the motion of the electrically conducting nanofluid as it approaches the surface of the stretching cylinder of the artificial kidney. It is noted from Figure 3 (b) that, an increase in Schmidt number (Sc) there is no significant decrease in radial velocity (Wr). It is noted from Figure 3 (c) that, the temperature of the nanofluid in the blood compartment decrease as Schmidt's number increases, but as it gets closer to the stretching cylinder's surface, it increases because the stretching cylinder serves as a heat source and hastens the distribution of solute particles from the blood through the hollow fiber pores in an artificial kidney. From Figure 3 (d) it is observed that an increase in Schmidt number causes an increase in concentration gradient by increasing the concentration boundary layer at the surface of the stretching cylinder. Blood with suspended nanoparticles has a higher Schimidtl-value, which reduces the mass diffusion rate and, hence, the concentration boundary layer thickness in the dialysis solution compartment.

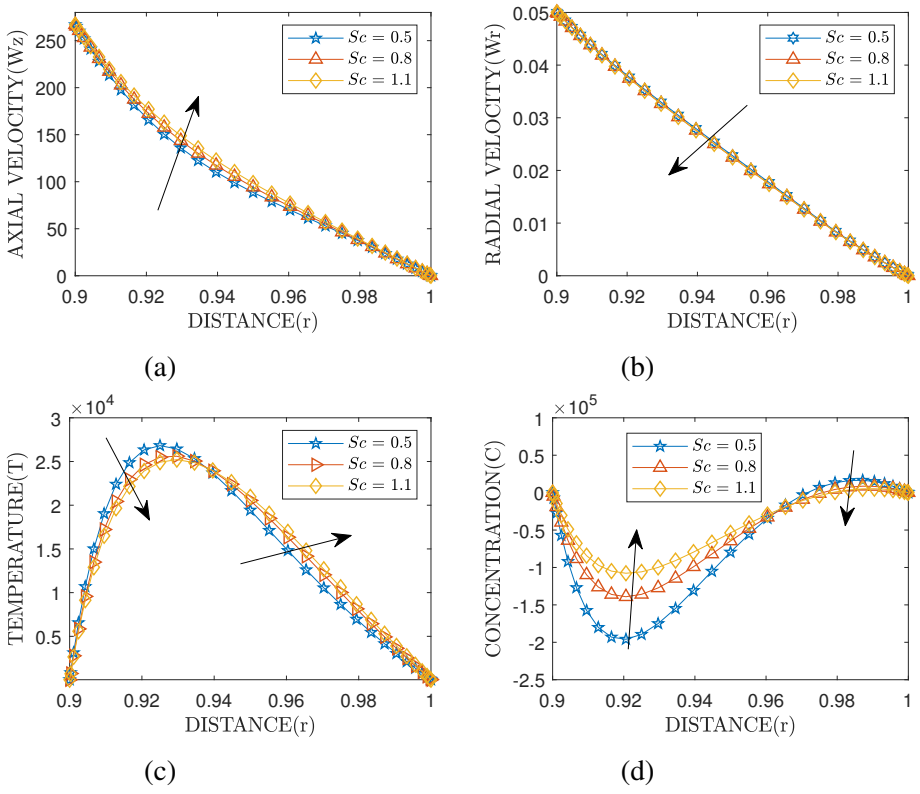

Figure 3: Effects of Schmidtl number(Sc) on Axial velocity (Wz), Radial velocity (Wr), Temperature (T) and Concentration (C) profiles

It is observed from the Figure $4\,(a)$ that as the Magnetic field parameter(M) increases the axial velocity (Wz) profile decreases, this is due to the Lorentz force generated by the applied magnetic field in the opposite direction to the electrically conducting nanofluid past porous stretching cylinder through hollow fibres in an artificial kidney which leads to decrease in velocity. From Figure $4\,(b)$ it is noted that the radial velocity (Wr) profile increases as Magnetic field parameter(M) increases. This is because the magnetic field is applied in the same direction as the radial distance. Figure $4\,(c)$ shows that an increase in applied magnetic field parameter(M) leads to an increase in temperature(T) profile in the blood compartment and decreases as it approaches the wall of the stretching cylinder of the dialysis solution compartment in an artificial kidney. Metallic nanoparticles used in the base fluid improve heat transfer on the thermal boundary layer, which leads to a higher temperature of the nanofluid. The temperature profile decreases as the magnetic field strength increases over the electrically conducting nanofluid. Lorentz force generated by magnetic force has the tendency to slow down the motion of base fluid, solutes, and any other metabolic products as well as controlling some of the electrolyte solution during blood filtration. From Figure $4\,(d)$ shows that an increase in the applied magnetic field leads to a decrease in the concentration profile in the blood compartment and increases exponentially as it approaches the dialysis solution compartment in an artificial kidney. Decreasing the velocity of nanofluid tends to improve the movement of solutes and other waste products from the blood during hemodialysis.

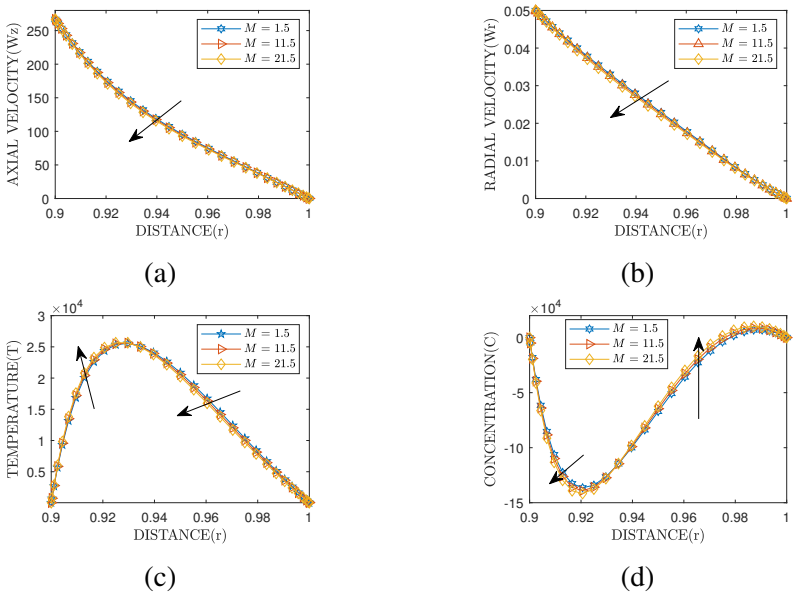

Figure 4: Effects of Magnetic field parameter (M) on Axial velocity (Wz), Radial velocity (Wr), Temperature (T) and Concentration (C) profiles

From Figure $5\,(a)$ it is observed that an increase in Prandtl number (Pr) results to

a decrease in nanofluid velocity (Wz). When heating is subjected to the mixture of nanoparticles and base fluid, heat diffuses relatively slow compared to velocity of the nanofluid as it is approaching the hollow fiber of the stretching cylinder that decelerates the nanofluid velocity. It is noted that in Figure $5\,(b)$an increase in Prandtl number (Pr) results to an increase in Radial velocity (Wr) profile. It is noted that as Prandtl number increases does not give significant change in nanofluid velocity since the increase in Prandtl number is approximately small to make significant as heat is applied in the mixture of base fluid and nanoparticles. Figure $5\,(c)$ shows that an increase in Prandtl number(Pr) leads to an increase in temperature(T) profile. It is to the fact that, the nanoparticles dissolved into base-fluid improves thermal conductivity of base-fluid where by ions of the basefluid moves faster through the pores of the hollow fibers of the stretching cylinder in the artificial kidney. Figure $5\,(d)$ shows that an increase in Prandtl number(Pr) leads to a decrease in concentration profile. This is because as the surface of the hollow tubes in the blood compartment in an artificial kidney becomes cooled, viscous force increases kinetic energy of the nanofluid particles. Hence concentration of the nanofluid increases past porous stretching plate.

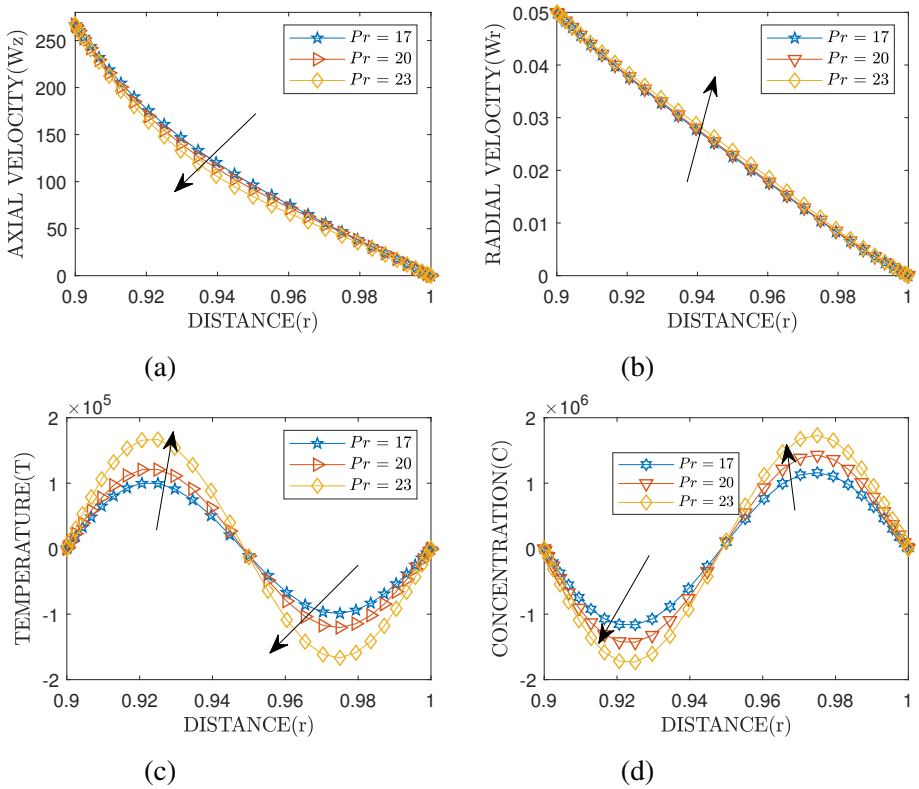

Figure 5: Effects of Prandtl number (Pr) on Axial velocity (Wz),Radial velocity (Wr),Temperature (T) and Concentration (C) profiles

It is observed from figure $6\,(a)$ that,as Joule heating parameter increases (H_J), axial

velocity (Wz) decreases. Change in temperature of nanofluid leads to a decrease in velocity boundary layer of the nanofluid particles that results to axial velocity profile to decrease. It is noted from figure $6\,(b)$ that, as Joule heating parameter(H_J) increases , Radial velocity (Wr) decreases, a decrease in Joule heating parameter has no significant effect on radial velocity since there is no temperature entry for the equation of motion in radial direction. It is noted from figure $6\,(c)$ that,as Joule heating parameter(H_J) increases temperature profile increases.The suspended nanoparticles in the base fluid, and heat generated from the stretching cylinder that acts as the heat source increases temperature distribution inside the hollow fibers of the blood compartment in an artificial kidney. From figure $6\,(d)$ it is observed that, as Joule heating parameter increases concentration profile decreases slowly until approaches the surface of stretching cylinder that acts as heat source helps solutes and other metabolic waste products to be filter out from blood to dialysis solution compartment.

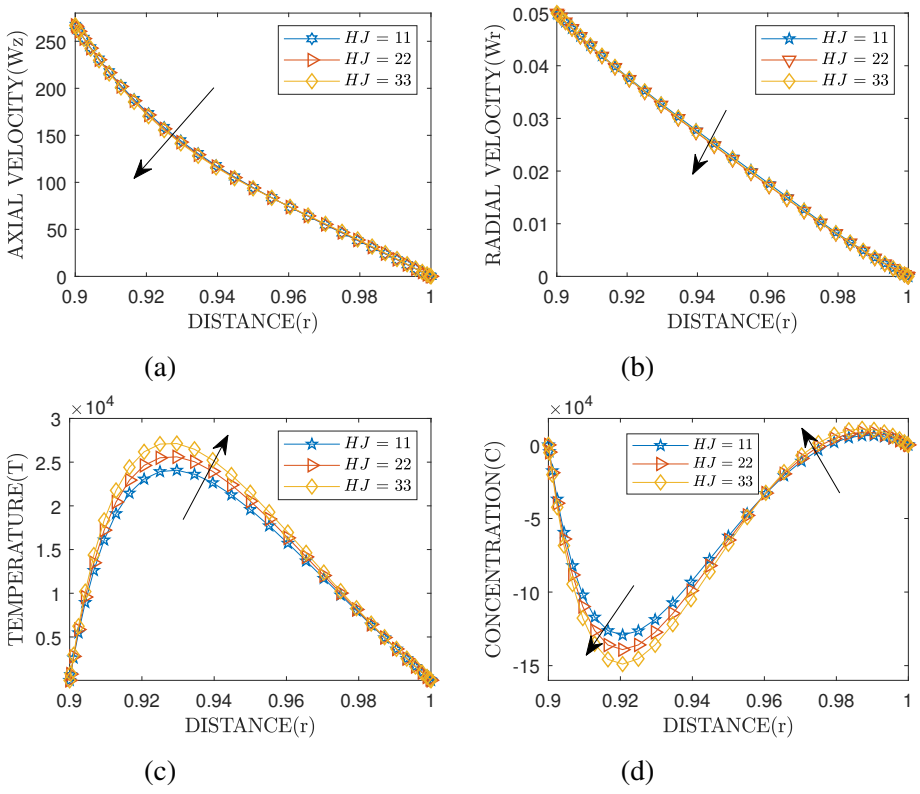

Figure 6: Effects of Joule heating parameter (H_J) on Axial velocity (Wz), Radial velocity (Wr), Temperature (T) and Concentration (C) profiles

Effects of Magnetic field(M), Permeability parameter(λ_p), Joule heating parameter(H_J), and time(t) on skin friction coefficient(C_s), heat transfer(Sh_m) and mass transfer(Nu_w) are given below

t	M	H_J	C_{s_z}	C_{s_r}	Sh_m	Nu_w
1.000	9.500	19.000	3.00175e+05	3.47217e+01	8.22154e+07	-9.75187e+06
2.000	9.500	19.000	2.09771e+05	1.17005e+02	2.08682e+07	-1.19064e+06
1.000	10.500	19.000	2.93023e+05	3.45077e+01	1.82312e+07	-2.62354e+06
1.000	9.500	19.000	2.93023e+05	3.45077e+01	1.82312e+07	-2.62354e+06
1.000	9.500	20.000	2.93023e+05	3.45077e+01	1.82312e+07	-2.62354e+06
1.000	9.500	19.000	2.93130e+05	3.45066e+01	1.83564e+07	-2.64050e+06

Table 1: Variation of various non-dimensional parameters on Skin friction coefficient, heat and mass transfer

From Table (1) one above

- It is observed that as t decreases both C_{s_z} and C_{s_r} , this increases velocity of nanofluid and solutes from blood through pores in membrane of the stretching cylinder. The values of Sh_m and Nu_w increases due to the application of nanoparticles suspended into base fluid and stretching cylinder acting as heat source improves mass transfer of solutes from blood to dialysis solution compartment during filtration.
- It is noted that an increase in M results in an increase in the values of C_{s_z} and C_{s_r} in magnitude due to an opposing force on nanofluid flow called Lorentz force. The values of Sh_m increases in magnitude and Nu_w decreases as M increases, this is due to the application of nanoparticles to base fluid that improves the thermal boundary layer thickness that helps solutes and other metabolic products from blood diffuse easily through pores of the stretching cylinder to the dialysis solution compartment.
- It is noted that an increases in H_J results to an increase in the values of C_{s_z} and the values of C_{s_r} increase in magnitude. The values of Sh_m increases in magnitude and the value of Nu_w decreases in magnitude as Joule heating parameter increases. Nanoparticles suspended into base fluid and heat dissipation into nanofluid improves hemodialysis of solutes and other metabolic products from blood to dialysis solution compartment in the artificial kidney.

4. CONCLUSION

The study of heat and mass transfer in hydromagnetic nanofluid convective flow through an artificial kidney past a porous stretching cylinder under the effects of thermal conductivity is considered by improving the natural kidney using hemodialysis conditions implemented by computer programming through simulation.

The following results have been observed as a resourceful way to increase the efficiency of an artificial kidney through time savings and practical cost effectiveness of the

hemodialysis session during blood filtration when varying different non-dimensional parameters with nanofluid velocity, temperature, and concentration profiles.

i When Pr, H_J, Sc, increase, causes an increase in axial velocity of nanofluid flow at the center of the blood compartment but decreases as it approaches the surface of the stretching cylinder of tyhe hollow fibres. When M, increases, results to the decrease of axial velocity.

ii. It is noted that M, Pr, H_J leads to an increase in the velocity of the solutes passing through the pores of hollow fibers at the surface of the stretching cylinder.

iii. It is observed that an increase in M, Pr, and H_J results to an increase in temperature in nanofluid flow and decreases when approaching the surface of the stretching cylinder.

iv. It is observed than an increase in, M, Pr, H_J results to a decrease in the concentration profile, and mass transfer of solutes increases at the surface of the stretching cylinder.

v. The application of nanoparticles into the base fluid improve thermal-conductivity that helps improving dialysis session during the filtration of patient's blood in an artificial kidney from a minimum of eight hours to one hour. Thus, as time decreases, the velocity of nanofluid, the velocity of solutes and other metabolic products from blood to dialysis solution, the temperature in the nanofluid flow and at the surface of the stretching cylinder, as well as the concentration gradient from the blood to the dialysis solution compartment, all improve.

5. DECLARATION OF CONFLICTING INTEREST

The authors declare that there are no special conflicts of interest shown by them that could disturb the whole process of writing this paper regarding cooperating in every step to make the work successful.

6. ACKNOWLEDGEMENT

The authors honestly do acknowledge that, no financial support when writing the research paper and publication of this paper.

NOMENCLATURE

Symbol	**Meaning.**
e	Unit electric charge(C) .
$\overrightarrow{E}$	Electric field (V).
$\overrightarrow{J}$	Current density (Am^{-2}).
$\overrightarrow{H}$	Magnetic field intensity vector (Am^{-1}).
ρ_c	Charge Density (Cm^{-3}).
$\overrightarrow{B}$	Magnetic field vector (Wbm^{-2}).
M	Magnetic field parameter.
D_m	Mass diffusivity coefficient (m^2s^{-1}).
$\overrightarrow{C}$	Concentration Vector (kgm^{-3}).
Re	Reynolds number parameter.
P	Force due pressure (Nm^{-2}).
$\overrightarrow{W}$	Velocity Vector of a fluid (ms^{-1}).
w_z	Axial velocity of the nanofluid in z-direction (ms^{-1})
w_r	Radial velocity of solutes through porous plate in r-direction (ms^{-1}).
i, j, k	Component Unit vectors in the x,y,z directions respectively.
u, v, w	Components of velocity vector $\overrightarrow{W}$ (ms^{-1}).
$u^\star, v^\star, w^\star$	Dimensionless velocity components.
r, θ, z	Dimensional cylindrical co-ordinates with position vector $\overrightarrow{p}$ (m).
$r^\star, \theta^\star, z^\star$	Dimensionless cylindrical polar co-ordinates.
F	Fluid Body force (Nm^{-3}).
g	Gravitational force $(kgms^{-2})$.
K_p	Darcy permeability (m^2).
$\overrightarrow{D}$	Displacement current density (Cm^{-2}) .
F_e	Electromagnetic force (kgm^2s^{-2}) .
Pr	Prandtl number.
λ_p	Permeability parameter.
Gr_T	Temperature Grashof number.
Gr_C	Concentration Grashof number.
C_s	Skin friction coefficient.
Sh_m	Sherwood number.
Nu_w	Nusselt number.

Ec	Eckert number.
H_J	Joule heating parameter.
Sc	Schmidtl number.
Sr	Soret number.
F_e	Electromagnetic force $(kgms^{-2})$.
$\frac{D}{Dt}$	Material derivative $\left(\frac{\partial}{\partial t}+u\frac{\partial}{\partial x}+v\frac{\partial}{\partial y}+w\frac{\partial}{\partial z}\right)$.
L	Dimensional length between plates of hollow fibres in an artificial kidney (m).
C	Dimensional concentration of solutes through hollow fibres (Kgm^{-3}).
C_s	Dimensional concentration at the stretching plate (Kgm^{-3}).
C_{R_2}	Dimensional concentration of the solutes at impermeable plate (Kgm^{-3}).
T	Absolute temperature of the nanofluid in an artificial kidney (K).
T_s	Absolute temperature at the stretching plate in an artificial kidney (K).
T_{R_2}	Absolute temperature at the impermeable plate in an artificial kidney (K).
c	stretching rate constant (s^{-1}).
C_f	Forchheimer dimensionless parameter.
β	Forchheimer Constant or inertia resistance coefficient (m).
C_p	Specific heat capacity at constant pressure $(Jkg^{-1}K^{-1})$.
S	Stretching parameter.
Sh_m	Sherwood number.
Nu_w	Nusselt number.
C_{s_z}	Wall skin friction coefficient in axial direction$(-)$.
C_{s_r}	Wall skin friction coefficient in Radial direction$(-)$.
Greek	**symbols**
e^+	Porosity
ρ_{nf}	Nanofluid density (kgm^{-3})
μ_{nf}	Coefficient of viscosity of nanofluid$(kgm^{-1}s^{-1})$
ν	Kinematic viscosity (m^2s^{-1})
β_T	Volumetric coefficient of thermal expansion (K^{-1})
β_C	Coefficient of thermal expansion due to concentration gradient (K^{-1})
ϕ	Viscous dissipation function $\left[\phi=\left(\frac{\partial V_i}{\partial x_j}+\frac{\partial V_j}{\partial x_i}\right)^2\right]$ (s^{-1})
σ	Electrical conductivity ,$(\Omega^{-1}m^{-1})$
μ_e	Magnetic permeability (Hm^{-1})
∇	Gradient operator $\left(\frac{\partial}{\partial x}i+\frac{\partial}{\partial y}j+\frac{\partial}{\partial z}k\right)$.
∇^2	Laplacian operator $\left(\frac{\partial^2}{\partial x^2}+\frac{\partial^2}{\partial y^2}+\frac{\partial^2}{\partial z^2}\right)$.
γ	Hemodialysis parameter.

REFERENCES

[1] Naveed Ahmad Khan and Muhammad Sulaiman. Heat transfer and thermal conductivity of magneto micropolar fluid with thermal non-equilibrium condition passing through the vertical porous medium. *Waves in Random and Complex Media*, pages 1–25, 2022.

[2] MA Aiyashi, Hassan Waqas, Faisal Fareed Bukhari, and Taseer Muhammad. A thermal model for bio-convection transport of nanofluid due to stretching cylinder with marangoni boundary conditions. *Waves in Random and Complex Media*, pages 1–17, 2022.

[3] Mehran Alavi, Mahendra Rai, Fleming Martinez, Danial Kahrizi, Haroon Khan, Irwin Rose Alencar De Menezes, Henrique Douglas Melo Coutinho, and José Galberto Martins Costa. The efficiency of metal, metal oxide, and metalloid nanoparticles against cancer cells and bacterial pathogens: different mechanisms of action. *Cellular, Molecular and Biomedical Reports*, 2(1):10–21, 2022.

[4] Mubashar Arshad, Azad Hussain, Ali Hassan, Syed Amir Ghazi Ali Shah, Mohamed Abdelghany Elkotb, Soumaya Gouadria, Mishal Alsehli, and Ahmed M Galal. Heat and mass transfer analysis above an unsteady infinite porous surface with chemical reaction. *Case Studies in Thermal Engineering*, 36:102140, 2022.

[5] Vikas Chaurasiya, Abderrahim Wakif, Nehad Ali Shah, and Jitendra Singh. A study on cylindrical moving boundary problem with variable thermal conductivity and convection under the most realistic boundary conditions. *International Communications in Heat and Mass Transfer*, 138:106312, 2022.

[6] Siping Ding, Tonghui Zhang, Peiyun Li, and Xuefen Wang. Dialysis/adsorption bifunctional thin-film nanofibrous composite membrane for creatinine clearance in portable artificial kidney. *Journal of Membrane Science*, 636:119550, 2021.

[7] Elsayed MA Elbashbeshy, Hamada Galal Asker, and Betty Nagy. The effects of heat generation absorption on boundary layer flow of a nanofluid containing gyrotactic microorganisms over an inclined stretching cylinder. *Ain Shams Engineering Journal*, 13(5):101690, 2022.

[8] M Gnaneswara Reddy, MVVNL Sudharani, MM Praveena, and K Ganesh Kumar. Effect of thermal conductivity on blasius–rayleigh–stokes flow and heat transfer over a moving plate by considering magnetic dipole moment. *The European Physical Journal Plus*, 137(1):1–13, 2022.

[9] Thomas Groth, Bernd G Stegmayr, Stephen R Ash, Janna Kuchinka, Fokko P Wieringa, William H Fissell, and Shuvo Roy. Wearable and implantable artificial

kidney devices for end-stage kidney disease treatment—current status and review. *Artificial Organs*, 2022.

[10] Keyvan Karimi and Mansour Rahsepar. Optimization of the urea removal in a wearable dialysis device using nitrogen-doped and phosphorus-doped graphene. *ACS omega*, 7(5):4083–4094, 2022.

[11] S Kavya, V Nagendramma, N Ameer Ahammad, Sohail Ahmad, CSK Raju, and Nehad Ali Shah. Magnetic-hybrid nanoparticles with stretching/shrinking cylinder in a suspension of mos4 and copper nanoparticles. *International Communications in Heat and Mass Transfer*, 136:106150, 2022.

[12] Tahir Saeed Khan, Ndolane Sene, Abir Mouldi, Ameni Brahmia, et al. Heat and mass transfer of the darcy-forchheimer casson hybrid nanofluid flow due to an extending curved surface. *Journal of Nanomaterials*, 2022, 2022.

[13] Najiyah Safwa Khashi'ie, Norihan Md Arifin, and Ioan Pop. Magnetohydrodynamics (mhd) boundary layer flow of hybrid nanofluid over a moving plate with joule heating. *Alexandria Engineering Journal*, 61(3):1938–1945, 2022.

[14] Pardeep Kumar, Hemant Poonia, Liaqat Ali, and Sujesh Areekara. The numerical simulation of nanoparticle size and thermal radiation with the magnetic field effect based on tangent hyperbolic nanofluid flow. *Case Studies in Thermal Engineering*, 37:102247, 2022.

[15] Matthew O Lawal, Kazeem B Kasali, Hammed A Ogunseye, Michael O Oni, Yusuf O Tijani, and Yussuff T Lawal. On the mathematical model of eyring–powell nanofluid flow with non-linear radiation, variable thermal conductivity and viscosity. *Partial Differential Equations in Applied Mathematics*, 5:100318, 2022.

[16] JK Madhukesh, BM Shankaralingappa, BJ Gireesha, and BC Prasannakumara. Evaluation of heat and mass transfer characteristics in a nanofluid flow over an exponentially stretchable sheet with activation energy. *Proceedings of the Institution of Mechanical Engineers, Part E: Journal of Process Mechanical Engineering*, page 09544089221074827, 2022.

[17] Sohail Nadeem, Wang Fuzhang, Fahad M Alharbi, Farrah Sajid, Nadeem Abbas, AS El-Shafay, and Fahad S Al-Mubaddel. Numerical computations for buongiorno nano fluid model on the boundary layer flow of viscoelastic fluid towards a nonlinear stretching sheet. *Alexandria Engineering Journal*, 61(2):1769–1778, 2022.

[18] Chetan Pandit, Arpita Roy, Suresh Ghotekar, Ameer Khusro, Mohammad Nazmul Islam, Talha Bin Emran, Siok Ee Lam, Mayeen Uddin Khandaker, and David Andrew Bradley. Biological agents for synthesis of nanoparticles and their applications. *Journal of King Saud University-Science*, 34(3):101869, 2022.

[19] Manfred Raff. *Mass Transfer Models in Membrane Processes: Applications in Artificial Organs*. Springer Nature, 2022.

[20] P Sudarsana Reddy, P Sreedevi, and Ali J Chamkha. Heat and mass transfer analysis of nanofluid flow over swirling cylinder with cattaneo–christov heat flux. *Journal of Thermal Analysis and Calorimetry*, 147(4):3453–3468, 2022.

[21] Muhammad Rooman, Muhammad Jameel, Asifa Tassaddiq, Zahir Shah, Ahmed Alshehri, and Poom Kumam. Significance of variable viscosity and thermal conductivity on the dynamics of mhd cross nanofluid over a stratified darcy-forchheimer porous surface of a paraboloid of revolution subjected to entropy generation. *International Communications in Heat and Mass Transfer*, 139:106464, 2022.

[22] Sina Sadighi, Mohsen Jabbari, Hossein Afshar, and Hossein Ahmadi Danesh Ashtiani. Mhd heat and mass transfer nanofluid flow on a porous cylinder with chemical reaction and viscous dissipation effects: Benchmark solutions. *Case Studies in Thermal Engineering*, page 102443, 2022.

[23] Ghulam Shah, Abdul Rehman, and Naveed Sheikh. Heat transfer analysis over the boundary layer stagnation-point flow of couple stress fluid over an exponentially stretching sheet. *American Journal of Applied Mathematics*, 10(3):100–105, 2022.

[24] M Shanmugapriya, R Sundareswaran, P Senthil Kumar, and Gayathri Rangasamy. Impact of nanoparticle shape in enhancing heat transfer of magnetized ternary hybrid nanofluid. *Sustainable Energy Technologies and Assessments*, 53:102700, 2022.

[25] Yu-Shuo Tang, Yu-Cheng Tsai, Tzen-Wen Chen, and Szu-Yuan Li. Artificial kidney engineering: The development of dialysis membranes for blood purification. *Membranes*, 12(2):177, 2022.

[26] Aqeel ur Rehman and Zaheer Abbas. Stability analysis of heat transfer in nanomaterial flow of boundary layer towards a shrinking surface: Hybrid nanofluid versus nanofluid. *Alexandria Engineering Journal*, 61(12):10757–10768, 2022.

[27] Christopher Venance, Mathew N Kinyanjui, Kang'ethe Giterere, et al. Effects of thermo-conductivity on hydromagnetic nanofluid convective flow through an

artificial kidney past a porous stretching cylinder. *Mathematical Problems in Engineering*, 2022, 2022.

[28] Wei-Feng Xia, Shafiq Ahmad, Muhammad Naveed Khan, Hijaz Ahmad, Aysha Rehman, Jamel Baili, and Tuan Nguyen Gia. Heat and mass transfer analysis of nonlinear mixed convective hybrid nanofluid flow with multiple slip boundary conditions. *Case Studies in Thermal Engineering*, 32:101893, 2022.

[29] Nusayba Yaseen, Feras Shatat, Firas A Alwawi, Mohammed Z Swalmeh, Muhammad Salman Kausar, and Ibrahim Mohammed Sulaiman. Using micropolar nanofluid under a magnetic field to enhance natural convective heat transfer around a spherical body. *Journal of Advanced Research in Fluid Mechanics and Thermal Sciences*, 96(1):179–193, 2022.

[30] Muhammad Yasir, Abdul Hafeez, and Masood Khan. Thermal conductivity performance in hybrid (swcnts-cuo/ehylene glycol) nanofluid flow: Dual solutions. *Ain Shams Engineering Journal*, 13(5):101703, 2022.

[31] Hammad Younes, Mingyang Mao, SM Sohel Murshed, Ding Lou, Haiping Hong, and GP Peterson. Nanofluids: Key parameters to enhance thermal conductivity and its applications. *Applied Thermal Engineering*, page 118202, 2022.

[32] Haixin Zhao, Jia Huang, Lu Miao, Yuqi Yang, Zuoxiu Xiao, Qiaohui Chen, Qiong Huang, and Kelong Ai. Toward urease-free wearable artificial kidney: Widened interlayer spacing mos2 nanosheets with highly effective adsorption for uremic toxins. *Chemical Engineering Journal*, 438:135583, 2022.